

UCSF

UC San Francisco Previously Published Works

Title

Inflammation Mediates the Development of Aggressive Breast Cancer Following Radiotherapy
Radiation-Preceded Breast Cancer

Permalink

<https://escholarship.org/uc/item/6nn6s5jv>

Journal

Clinical Cancer Research, 27(6)

ISSN

1078-0432

Authors

Ma, Lin

Gonzalez-Junca, Alba

Zheng, Yufei

et al.

Publication Date

2021-03-15

DOI

10.1158/1078-0432.ccr-20-3215

Peer reviewed

Inflammation mediates development of aggressive breast cancer following radiotherapy

Lin Ma¹, Alba Gonzalez-Junca¹, Yufei Zheng^{1,2}, Haoxu Ouyang^{3,4}, Irineu Illa-Bochaca^{3,5}, Kathleen C. Horst⁶, Gregor Krings⁷, Yinghao Wang^{1,8}, Ignacio Fernandez-Garcia^{3,9}, William Chou¹ and Mary Helen Barcellos-Hoff¹⁺

¹ Department of Radiation Oncology and Helen Diller Family Comprehensive Cancer Center, University of California, San Francisco, 2340 Sutter Street, San Francisco, CA 94115, USA

² Current address: College of Animal Sciences, Zhejiang University, Hangzhou 310027, China

³ Department of Radiation Oncology, New York University School of Medicine, 566 First Avenue, New York, NY 10016, USA

⁴ Current address: Department of Medicine, Kingsbrook Jewish Medical Center, 585 Schenectady Ave, Brooklyn, NY 11203, USA

⁵ Current address: The Ronald O. Perelman Department of Dermatology, New York University School of Medicine, 522 1st Avenue, Smilow 403, New York, NY 10016, USA

⁶ Department of Radiation Oncology, Stanford University School of Medicine, Stanford, CA 94305, USA

⁷ Department of Pathology, University of California, San Francisco, 1825 4th Street, San Francisco, CA 94158, USA

⁸ Current address: Department of Biomedical Engineering, College of Engineering, University of Michigan, Carl A. Gerstacker Building, 2200 Bonisteel Blvd, Ann Arbor, MI 48109, USA

⁹ Current address: F. Hoffmann-La Roche Ltd, Basel, CH 4070, Switzerland

+Corresponding Author:

Mary Helen Barcellos-Hoff, Ph.D.
Department of Radiation Oncology
Helen Diller Family Comprehensive Cancer Center
University of California, San Francisco
2340 Sutter St., San Francisco, CA 94143
MaryHelen.Barcellos-Hoff@ucsf.edu

Conflicts of Interest: The authors declare there are no conflicts of interest regarding these data.

Key Words: ionizing radiation, breast cancer, tumor microenvironment, inflammation, aspirin

Running Title: Radiation-preceded breast cancer

Word count: 6035, introduction through discussion

Abbreviations: tumor microenvironment, TME; immunosuppressive TME, iTME; triple-negative breast cancer, TNBC; transforming growth factor β , TGF β ; radiation-preceded breast cancer, RP-BC; interferon γ , IFN γ ; cyclooxygenase 2, COX2; Hodgkin's lymphoma, HL; tumor infiltrating lymphocytes, TIL.

References: 69

Figures: 6

Supplementary Tables: 3

Supplementary Figures: 7

Translational relevance

Women treated with radiation therapy for cancer before the age of 30 have a substantial risk of developing early breast cancer, similar to that of women of the same age with *BRCA1* germline mutations. We found that compared to sporadic breast cancer, radiation-preceded breast cancers are characterized by a markedly immunosuppressive tumor microenvironment. We used a murine mammary carcinogenesis model to dissect the contribution of host response to radiation. The immunosuppressive tumor microenvironment was recapitulated in irradiated mice as a function of innate immunity. Aspirin treatment shortly after irradiation shifted carcinogenesis toward a less immunosuppressive tumor microenvironment, implicating radiation induced low grade inflammation in its genesis.

Abstract

Purpose: Women treated with radiotherapy before 30 years of age have increased risk of developing breast cancer at an early age. Here we sought to investigate mechanisms by which radiation promotes aggressive cancer.

Experimental Design: The tumor microenvironment (TME) of breast cancers arising in women treated with radiotherapy for Hodgkin's lymphoma was compared to that of sporadic breast cancers. We investigated radiation effects on carcinomas arising from *Trp53* null mammary transplants after irradiation of the target epithelium or host using immunocompetent and incompetent mice, some which were treated with aspirin.

Results: Compared to age-matched specimens of sporadic breast cancers, radiation-preceded breast cancers were characterized by TME rich in transforming growth factor β , cyclooxygenase-2 and myeloid cells, indicative of greater immunosuppression, even when matched for triple-negative status. The mechanism by which radiation impacts TME construction was investigated in carcinomas arising in mice bearing *Trp53* null mammary transplants. Immunosuppressive TME (iTME) were recapitulated in mice irradiated before transplantation, which implicated systemic immune effects. In Nu/Nu mice lacking adaptive immunity irradiated before *Trp53* null mammary transplantation, cancers also established an iTME, which pointed to a critical role for myeloid cells. Consistent with this, irradiated mammary glands contained more macrophages and human cells co-cultured with polarized macrophages underwent dysplastic morphogenesis mediated by interferon γ . Treating mice with low-dose aspirin for 6 months post-irradiation prevented establishment of an iTME and resulted in less aggressive tumors.

Conclusions: These data show that radiation acts via non-mutational mechanisms to promote markedly immunosuppressive features of aggressive, radiation-preceded breast cancers.

Introduction

Women successfully treated with radiotherapy before 30 years of age in which the chest is exposed have significantly increased risk of breast cancer (1). The cumulative incidence of early breast cancer, i.e. by 45 years of age, is 13–20%, similar to the 10–19% incidence in women with a *BRCA* germline mutation, and substantially higher than 1% evident in the general population (2). Moreover, radiation-preceded breast cancer (RP-BC) is more likely to be hormone receptor negative (3) compared to sporadic breast cancer (sporadic-BC), and to exhibit gene expression profiles indicative of more aggressive cancers (4). Horst and colleagues reported that compared with age-matched, sporadic-BC, women treated with radiation for Hodgkin's lymphoma (HL) are significantly more likely to be diagnosed with triple-negative breast cancer (TNBC) lacking hormone receptors and human epidermal growth factor receptor 2 (HER2), which has a poorer prognosis compared to more prevalent hormone receptor positive cancer (5). Childhood cancer survivors indicate that these patients have worse outcomes, regardless of breast cancer type (6,7).

Radiation as a carcinogen is typically considered through the prism of cell intrinsic effects, i.e. DNA damage results in mutations that occasionally initiate transformation, yet stochastic mutational events are unlikely to explain the high rate of TNBC histology in RP-BC. Radiation exposure also dysregulates multiple tissue processes in which cells other than those with oncogenic mutations influence the frequency and characteristics of subsequent cancer (8). Murine breast cancer models have shown that changes in the irradiated tissue microenvironment affects carcinogenic potential via specific signals or broad systemic effects (9,10). An example of the former is activation of transforming growth factor β (TGF β), a potent cytokine that mediates extracellular matrix remodeling and stem cell fate decisions (11,12), whereas the latter is exemplified by chronic, low-level inflammation that can lead to a cycle of subclinical tissue damage (13).

Cancer evolves dynamically; cell-intrinsic genomic changes initiate malignancy in the context of highly regulated tissue processes that suppress tumor development but eventually give way to support cancer by forming a mature tumor microenvironment (TME) (8). In parallel, malignancy is opposed by systemic immune surveillance that initially eliminates and edits malignant cells, and whose ultimate failure is prerequisite for clinically evident cancer (14). Notably, immune escape results in three patterns of lymphocytic infiltration: desert tumors that are devoid of lymphocytic infiltrates, excluded tumors in which lymphocytes are restricted to the interface of parenchyma and tumor, and inflamed tumors in which tumor infiltrating lymphocytes (TIL) are ineffective to control tumor growth (15). In breast cancer, the presence of TIL correlates with patient prognosis (16). The spatial distribution of cytotoxic T cells tumor-infiltration also has prognostic significance and is predictive of response to non-immunotherapy (17,18). Thus, a growing body of literature supports modeling carcinogenesis not only as the sum of malignant mutations but as a consequence of its TME composition, which is constructed in response to variable tissue factors and immune surveillance that together ultimately determine therapeutic response (19).

Here we report that compared to age-matched, sporadic-BC, the TME of RP-BC is enriched in pro-inflammatory factors and abundant myeloid cells. To investigate the mechanism by which

radiation exposure mediates construction of this highly immunosuppressive TME (iTME), we evaluated radiation effects on the target epithelium, host biology and immune system using a mammary chimera model in which mice are transplanted with *Trp53* null mammary epithelium. Mammary cancers arising in irradiated mice exhibit the iTME that characterized RP-BC; these tumors also grew considerably faster. Notably, this radiation effect was not dose dependent and did not require that the target epithelium be irradiated, implicating systemic responses to radiation exposure. We next conducted the experiment in Ncr nude mice that lack effective cytotoxic lymphocytes. Surprisingly, adaptive immunity was not required to establish the iTME or increase growth rate, which pointed to innate immunity as a driver. This premise was tested by co-culturing non-malignant human breast epithelial cells with differentiated macrophages, whose production of TGF β and interferon γ (IFN γ) potentiated epithelial dysplasia. These data prompted us to test whether a common anti-inflammatory, aspirin, could ameliorate the effect of radiation in immunocompetent mice. A short course of aspirin after irradiation and before tumors developed reset the TME and decreased tumor growth rate of tumors arising in irradiated hosts. Thus, radiation exposure acts via inflammation, a non-mutational mechanism that promotes more aggressive cancers.

Materials and Methods

Human breast cancer specimens: Sections from formalin-fixed, paraffin-embedded (FFPE) of RP-BC and aged matched sporadic-BC with recorded estrogen receptor, progesterone receptor and HER2 status were collected from Stanford University pathology core and UCSF pathology department (Supplementary Table 1).

Mice: Experiments conducted at New York University used BALB/c wild type mice (3-week old, female) purchased from the Jackson Laboratory (Bar Harbor, ME) and were irradiated with a Cs¹³⁷ source γ -ray irradiator at NASA Space Radiation Laboratory at Brookhaven National Lab. Experiments conducted at UCSF Mt. Zion with approval of the animal welfare committee and using Ncr nude athymic mice (4-week old, female) purchased from Taconic (Albany, NY) or BALB/c wild type mice (3-week old, female) purchased from the Jackson Laboratory (Sacramento, CA) were irradiated whole body to the indicated dose with a Cs¹³⁷ γ -ray source. All mice were housed five per cage, fed with Lab Diet 5008 chow and water *ad libidum*. Experiments were approved by the institutional animal welfare committee.

Mammary Chimera Model: The mammary chimera model was established as previously described (1). In brief, the epithelium of both inguinal glands was surgically removed (i.e. cleared) from 3-week old BALB/c mice or 4-week old Ncr nude mice. Mice were randomly assigned into treatment groups based on body weights. In the genetic chimera model, *Trp53* null fragments were transplanted concomitant with clearing and the mice were whole body irradiated at 10 weeks of age with 10, 50, or 100 cGy γ -ray. In the radiation-genetic chimera model, the mammary glands of BALB/c wild type and Ncr nude mice were cleared and mice aged to 10 weeks before irradiation (50 or 100 cGy for BALB/c mice, 10 cGy for Nude mice). Three days after irradiation, both inguinal fat pads were transplanted with *Trp53* null fragments from 10-week old *Trp53* null BALB/c mice bred inhouse under similar conditions. Simultaneous sham-irradiated mice served as controls in each experiment. For aspirin treatment, drinking water containing 0.1 mg/ml aspirin, refreshed weekly, was provided for 6 months. Each mouse

consumed approximately 4 ml water a day, thus the aspirin dose was approximately 0.4 mg/day. Based on body surface area conversion (2), this dose is similar to human dose for 100 mg/day.

A subset of randomly selected mice were collected for analysis at 3-4 months after irradiation. Otherwise mice were monitored for 500 days by palpation weekly, then three times a week after a tumor were detected. Palpable tumors were measured using calipers until the tumor reached approximately 500 mm³ (e.g. 10 mm width, 10 mm length). Survival surgery was used to collect the first mammary tumor to allow tumor generation in the contralateral fat pad. Harvested tumors were cut into 3 pieces, one was frozen in liquid nitrogen, one embedded and frozen in O.C.T. (Sakura Tissue-Tek) and one was formalin fixed followed by paraffin embedding. The mouse was further observed until the resected tumor recurred, at which point the mouse was euthanized, or until the contralateral fat pad developed a tumor, which was monitored as above. A gross necroscopy was performed upon termination. If no tumor developed by experiment termination, then an inguinal gland wholemount was prepared to determine successful transplantation; mammary fat pads in which transplantation failed were censored. An informative transplant was defined as that which had an epithelial outgrowth evident by tumor development or outgrowth at sacrifice at experiment termination. Mouse palpation, tumor measurement and collection were conducted by technicians who were blind to the treatment groups.

Opal multiplexing staining: FFPE sections were deparaffinized with xylene (Sigma, Cat#214736) and rehydrated with a decreasing gradient of alcohols, followed by Antigen Unmasking Solution (Vector Laboratories, Cat#H-3300 or Cat#H-3301) and the Opal 7-color kit (Akoya, Cat#NEL811001KT) were used according to manufacturer instructions. Endogenous peroxidase was quenched by 3% hydrogen peroxide in PBS (diluted from 30% hydrogen peroxide, Sigma Cat#H1009). Each section passed through four to six sequential rounds of staining (Supplementary Table 2). Each round consisted of a protein block with 0.5% casein (Spectrum, Cat#CA205) in TN buffer (0.1 M Tris-HCl, 0.15 M NaCl) for 1 hour at room temperature, a primary antibody overnight incubation at 4°C, a corresponding secondary HRP-conjugated polymer incubation for 1 hour at room temperature, and a 10-minute incubation for each HRP-conjugated polymer, which mediated the covalent binding of a different fluorophore using tyramide signal amplification for each primary and secondary antibodies listed in Supplementary Table 2. An additional antigen retrieval using heated citric acid buffer (pH 6.0) for 15 minutes was then used to remove bound antibodies before the next step in the sequence. After all sequential reactions, sections were counterstained with spectrum appropriate 4',6-diamidino-2-phenylindole (DAPI) (Akoya, Cat#NEL811001KT) and mounted with Vectashield Hard Set mounting medium (Vectashield, Cat#H-1400).

Opal stained sections were imaged using the Vectra Multispectral Imaging System version 2 (Akoya) and analyzed by inForm 2.1 (Akoya). Single stained slides for each marker and associated fluorophore were used to establish the spectral library, which helped to separate the individual marker from the multiplexing image cube. For each marker, positive cells were determined based on the mean fluorescent intensity per case. The inForm 2.1 trainable tissue segmentation algorithm (Akoya) was used to segment tumor and stromal regions based on the markers and DAPI stained nuclear shape. The percentage of positive cells for each marker in the

region designated tumor or stroma were analyzed separately by the score algorithm in 3 to 5 random images taken under 20× objective.

Images of whole sections were used for CD8 pattern analysis. Tumors were classified into three patterns of CD8+ T-cell infiltrate of tumors as previously described (3). In brief, infiltrated tumors contain well-distributed CD8+ cells, excluded tumors are characterized by a dense accumulation of CD8+ cells at the tumor stroma, whereas tumors defined as deserts have few CD8+ cells, as shown in Fig. 1A.

Immunofluorescence: FFPE sections were deparaffinized and rehydrated as above. Citrate antigen unmasking (Vector Antigen unmasking solution, Vector Laboratories, Cat#H-3300) was performed before blocking with 0.5% casein/PBS. Primary antibody for Ki67 (ThermoFisher/Live Vision, Cat#RM9106-S1, RRID:AB_149792), pSmad2 (Cell Signaling, Cat#3108, RRID:AB_490941), CD8 (ThermoFisher, Cat#14-0808-80, RRID:AB_2572860), CD3e (ThermoFisher, Cat#MA514524, RRID:AB_10982026), CD11b (abcam, Cat#ab133357, RRID:AB_2650514), Gr1 (R&D, Cat#MAB1037, RRID:AB_2232806), wide spectrum cytokeratin (abcam, Cat#ab9377, RRID:AB_307222), cleaved caspase 3 (Cell Signaling, Cat#9661S, RRID:AB_2341188), COX2 (abcam, Cat#ab15191, RRID:AB_2085144) and TGFβ (R&D, Cat#AF101-NA, RRID:AB_354384) were diluted in 0.5% casein/PBS and incubated overnight at 4°C. The slides were washed three times with 0.1% Tween20/PBS. Secondary antibodies conjugated with fluorochrome were used to visualize the respective primary antibodies. DAPI (ThermoFisher, Cat#D1306) was used as nuclear counterstaining.

Natural killer marker CD335 was analyzed using 5 μm cryosections postfixed using 4% paraformaldehyde for 20 minutes at room temperature, specimens were blocked with 0.5% casein/PBS and incubated with anti-CD335 (BioLegend, Cat#137601, RRID:AB_10551441) diluted in 0.5% casein/PBS overnight at 4°C, followed by washes with 0.1% Tween 20/PBS and incubation with Alexa Fluor-488 Donkey anti-rat (Invitrogen, Cat#A21208, RRID:AB_141709) secondary antibodies diluted in blocking buffer for 1 hour at room temperature. Specimens were counter-stained with DAPI.

Specimens were imaged using a 20X Zeiss Plan-Apochromat objective with 0.95 numerical aperture on a Zeiss Axiovert epifluorescent microscope. All images were acquired with a CCD Hamamatsu Photonics monochrome camera at 1392 X 1040-pixel size, 12 bits per pixel depth. All images were assembled as false-color images using the Metamorph imaging platform (Molecular Devices, Inc.). Three to five random images were taken for each tumor. Positive cells per high-power field (HPF) were manually counted. For COX2 and TGFβ, mean intensities for each HPF image was measured by an inhouse ImageJ (ImageJ, RRID:SCR_003070) program (20).

Immunohistochemistry: FFPE mammary gland sections were deparaffinized, rehydrated, and exposed to citrate antigen unmasking (Vector Laboratories, Cat#H-3300) before blocking with 0.5% casein/PBS. Endogenous peroxidase was quenched by 3% hydrogen peroxide in PBS. Primary antibody for F4/80 (ThermoFisher, Cat#MA5-16363, RRID:AB_2537882) was diluted in 0.5% casein/PBS and incubated overnight at 4°C. The slides were washed three times with 0.1% Tween20/PBS. Secondary antibody conjugated with HRP (ThermoFisher, Cat#31466, RRID:AB_10960844) was incubated for 1 hour at room temperature. After washing with 0.1%

Tween20/PBS, incubated for 5 minutes with 3, 3' diaminobenzidine (Sigma, Cat# D8001) and counterstained with hematoxylin (Sigma, Cat#GHS232). Sections were dehydrated through graded alcohols, cleared in Xylene and mounted in Permount (Fisher scientific, Cat#SP15). Three random bright field images per section were taken using a 10X objective with 0.95 numerical aperture and F4/80+ positive cells per HPF were manually counted.

Cell culture: Nonmalignant human mammary epithelial cell line, MCF10A (ATCC, Cat#CRL10317, RRID:CVCL_0598) and transformed cell line MCF10A (MCF10DCIS.com, RRID:CVCL_5552) were cultured following ATCC recommendations in MGEM culture media (Lonza, CAT#CC-3150). Monthly mycoplasma testing was performed on both cell lines. Cells were maintained at low density, changing the media every other day. Cells were irradiated (25 cGy) 48 hours after seeding using a Cs¹³⁷ source γ -ray irradiator.

Macrophage were differentiated in vitro as described (21). In brief, buffy coats from healthy volunteer donors were obtained from the New York City Blood Bank at Long Island (Queens, NY). PBMC were separated immediately by density gradient using Ficoll-Paque (GE Healthcare, Cat#45001749). CD14+ monocytes were isolated using CD14 MicroBeads (Miltenyi Biotech, Cat#130-050-201) following manufacturer's instructions. The resulting monocytes were cultured with PromoCell Macrophage Generation Media (PromoCell, Cat#C-28055) for the generation of undifferentiated (M0), classically activated (M1) and alternatively activated (M2) macrophages. 7 days after, macrophages were activated with lipopolysaccharide (LPS, Sigma Aldrich, Cat#L4391) and IFN γ (R&D, Cat#258-IF-100) for M1 or with IL-4 (R&D, Cat#204-IL-010) and TGF β (500 pg/ml, R&D, Cat#240-B-002) for M2. 48 hours after, macrophages were collected using the macrophage detachment solution (PromoCell, Cat#C-41330), counted and added to sham or irradiated MCF10A cells in combination with TGF β (400 pg/ml) and/or anti-IFN γ naturalizing antibody (abcam, Cat#ab25101, RRID:AB_448613).

Macrophages were stained with fluorescent-labeled human antibodies: APCCy7-CD45 (BioLegend, Cat#304014, RRID:AB_314402), PerCP-Cy5.5-CD14 (BioLegend, Cat#325622, RRID:AB_893250), APC-CD68 (BioLegend, Cat#333809, RRID:AB_10567107), Pacific Blue-CD11b (BioLegend, Cat#301315, RRID:AB_493015), FITC-CD80 (ThermoFisher, Cat#11-0809-41, RRID:AB_10854884), PE-CD163 (BioLegend, Cat#333605, RRID:AB_1134005), and Violet Bright 711-IFN γ (BioLegend, Cat#502540, RRID:AB_2563506). Yellow Live/Dead fixable reagent (Life Technologies, Cat#L-34959) was used to discard dead cells from the analysis. Macrophage subtypes were analyzed by a BDLSRII Cytometer (Beckman Dickinson) and populations were quantified using FlowJo v8 (FlowJo, RRID:SCR_008520).

To assay MCF-10A 3-dimensional morphogenesis, co-cultures of MCF10A epithelial cells and macrophages were trypsinized 7 days after treatment and stained with human APC-Cy7-CD45 antibody (BioLegend, Cat#304014, RRID:AB_314402). Propidium iodide (Fisher, Cat#P3566) was used to exclude dead cells. Epithelial cells negatively sorted from co-cultures were seeded on top of Matrigel (Corning, Cat#356231). Media was supplemented with 2% Matrigel and human EGF (Life Technologies, Cat#PHG-0311) every other day. Cultures were imaged after 15 days. Representative images were taken by 10X objective in bright phase on a Nikon Diaphot 200 microscope with a 5 MP C-Mount Camera ZC505 (Zarbeco). The area and perimeter of each acini was quantified using ImageJ. The shape factor is defined as $P^2/(4\pi A)$, where P is the

perimeter and A is the area of the colony. This value is equal to 1 for a perfect circle. A value of >1 is interpreted as the amount of deformation in comparison to a circle. MCF10ADCIS.com were used as a positive control for aberrant morphogenesis.

qRT-PCR: Macrophages polarized using different conditions were lysed using RNA lysis buffer (QIAzol Lysis Reagent, Qiagen, Cat#79306) and stored at -80°C. RNA was extracted following manufacturer's instructions (RNeasy mini kit, Qiagen, Cat#74104). cDNA was generated from RNA using the SuperScript™ III kit (ThermoFisher, Cat#18080093) and following manufacturer's instructions. GAPDH and RPL13 were used as housekeeping internal controls for gene-expression normalization. Quantitative real-time PCR (qRT-PCR) was performed with SYBR green (ThermoFisher, Cat#4309155) and the following primers (Eurofins Scientific):

IFNG-Forward primer sequence: GGCATTTTGAAGAATTGGAAAG

IFNG-Reverse primer sequence: TTTGGATGCTCTGGTCATCTT

GAPDH- Forward primer sequence: CAGCCTCCAGATCATCAGCA

GAPDH- Reverse primer sequence: TGTGGTCATGAGTCCTTCCA

RPL13- Forward primer sequence: CAGCGGCTGAAGGAGTACC

RPL13- Reverse primer sequence: GGTGGCCAGTTTCAGTTCTT

Statistical Analysis: Statistical analysis was performed using Prism (GraphPad Prism, RRID:SCR_002798). Tumor growth curves were plotted for independent treatment group to an exponential curve and averaged, statistics were tested by Fisher-test. Comparison between sham and IR groups were tested by unpaired t-test (for normal distributions) or Mann-Whitney test (for nonparametric variables). Comparison among sham and IR groups with or without aspirin intervention were tested by one-way ANOVA. P value < 0.05 was considered statistically significant.

Results

The TME of RP-BC is more immunosuppressive than that of sporadic-BC.

We analyzed FFPE sections of age-matched, RP-BC (n=22) and sporadic-BC (n=43) specimens. The RP-BC patient characteristics are summarized in Supplementary Table 1 and 2. The mean age at first cancer treatment with radiation was 28.4 +/- 9.7 years; the mean age at breast cancer diagnosis was 47.3 +/- 10.1 years. Approximately half of each group was classified as TNBC by markers (RP-BC, 10/22; sporadic-BC, 23/43). TIL are a strong prognostic marker in early-stage TNBC (22). Moreover, our recent experimental studies indicated that mammary tumors arising in irradiated mice shifted from predominantly inflamed to deserts (20). Therefore, we performed CD8 immunofluorescence staining and classified the breast cancers according to three infiltrate patterns: inflamed (abundant CD8⁺ TIL), excluded (presence of CD8⁺ T cells at the perimeter), and desert (absence of CD8⁺ T cells). 43% of RP-BC were classified as immune desert tumors. In contrast, more than half (56%) of sporadic-BC was the inflamed phenotype (**Fig. 1A**).

To further characterize the TME in these specimens, we used multiplex immunostaining to simultaneously identify inflammatory factors and immune cell markers (Supplementary Fig.

1A). Compared to sporadic-BC, RP-BC exhibited higher expression of stromal cyclooxygenase 2 (COX2; **Fig. 1B**), which has both local and systemic effects (23), particularly in cancer progression and response to therapy (24). Expression of programmed death ligand-1 (PD-L1) delivers an inhibitory signal that impairs T cell function and promotes tumor immune escape (25). RP-BC exhibit more PD-L1 (**Fig. 1C**). Radiation elicits remarkably persistent changes in gene expression that are TGF β dependent and associated with inflammation (26). RP-BC were also characterized by abundant TGF β (**Fig. 1D**), which is a potent suppressor of anti-tumor immunity (27). Cells marked by a common myeloid lineage marker, CD11b, were more frequent in RP-BC (**Fig. 1E**). In contrast, sporadic-BC had fewer CD11b⁺ cells and more CD4⁺ and CD8⁺ TIL (**Fig. 1F-G**).

Because RP-BC are enriched in TNBC (5), we then specifically compared TNBC. COX2, PD-L1, TGF β and CD11b⁺ cells were still significantly elevated in RP-BC TNBC compared to sporadic-BC (Supplementary Fig. 1B-E), whereas CD4 and CD8 TIL were significantly reduced (Supplementary Fig. 1F,G). Together, these features of RP-BC constitute a more immunosuppressive TME compared to those of sporadic-BC.

Cancer arising in the irradiated genetic chimera model recapitulate the iTME of RP-BC.

To investigate how radiation exposure contributes to the TME composition, we used the *Trp53* null genetic chimera model in which the cleared fatpads of wildtype mice are transplanted with *Trp53* null mammary epithelium. Transplants rapidly generate full mammary ductal outgrowths that eventually give rise to diverse carcinomas in late life (28). Our prior publications have shown that *Trp53* null outgrowths give rise to palpable carcinomas that are diverse by all criteria, markers, histology, metastatic capacity and genomic profiling, and that radiation alters the breast cancer spectrum (20,26[Nguyen, 2013 #18373,29]). In this experiment, we evaluated the effect of graded doses of radiation to affect the features identified in RP-BC. Three-week old mice were surgically cleared of endogenous mammary gland and simultaneously transplanted with *Trp53* null mammary gland fragments (**Fig. 2A**). Mice were aged to 10 weeks of age (young adult), which emulates 20-30 year-old-humans, and irradiated whole body with graded doses of γ -radiation. Irradiated mice developed more mammary cancers (Supplementary Fig. 2A, B, D and E) and arose with a shorter latency (Supplementary Fig. 2C, F) compared to tumors arising in sham-irradiated mice. Breast cancers in HL cancer survivors treated with radiotherapy also occur at a younger age than the general population (5). Once detected, tumors arising in irradiated mice grew faster than those in sham mice (**Fig. 2B**; Supplementary Fig. 3A, B). Our prior studies suggest that tumor growth rate is largely determined by the composition of lymphocytic immune infiltrate, i.e. highly infiltrated tumors grow slowly due to an active yet insufficient immune response (20).

As observed in human breast cancers, tumors from irradiated mice were characterized by a markedly iTME. As compared to tumors from sham-irradiated mice, COX2 and TGF β expression was higher (**Fig. 2C,D**). More CD11b⁺ myeloid cells were present (**Fig. 2E**), which were also Gr1⁺ (**Fig. 2F**). Furthermore, tumors from irradiated mice had fewer tumor-infiltrating CD3⁺ and CD8⁺ T cells, and less apoptotic cells compared to tumors from sham mice (**Fig. 2G-I**). Thus, radiation exposure in this murine model recapitulates development of cancers with a highly iTME.

Radiation induced tumor immune features are mainly regulated by radiation effects on the host.

In the genetic chimera model, mice were irradiated after transplantation, i.e. cancers arose from an irradiated *Trp53* null epithelium in the context of an irradiated wildtype tissue and host. To evaluate the relative contribution of host response to radiation, we used the radiation-genetic chimera in which the mice were irradiated prior to transplantation (i.e. the transplanted mammary epithelium was not irradiated), which separates the effects of radiation on the host from those that directly affect target tissue, e.g. malignant mutations (**Fig. 3A**). In contrast to the irradiated genetic chimera, in which tumor frequency increased and latency decreased, tumor frequency and latency were not significantly different between radiation-genetic chimera and that of sham hosts (Supplementary Fig. 2D-F). These data are consistent with the hypothesis that misrepair of radiation-induced DNA damage increased initiation by oncogenic mutations.

However, tumors arising in irradiated hosts still exhibit faster growth rate compared to tumor from sham-irradiated hosts (**Fig. 3B**; Supplementary Fig. 3C,D). Notably, tumors from irradiated hosts also displayed immunosuppressive features, including higher COX2 and TGF β expression (**Fig. 3C,D**), more CD11b⁺ myeloid cells (**Fig. 3E**) and more CD11b⁺/Gr1⁺ myeloid cells (**Fig. 3F**) and were less infiltrated by CD3⁺ and CD8⁺ cytotoxic T cells (**Fig. 3G,H**). Consistent with decreased presence of cytotoxic T cells, fewer apoptotic cells were evident in tumors arising in irradiated mice (**Fig. 3I**). As host irradiation was sufficient to recapitulate critical immune features of RP-BC, and the differential immune cell infiltrate implicated adaptive immunity, we postulated that radiation affected anti-tumor immunity, which in turn influenced the development of an iTME.

The iTME is established in the absence of cytotoxic T cells. Given this perspective, we next evaluated the contribution of the immune system in the formation of *Trp53* null mammary tumors by using Ncr nude mice that lack an effective cytotoxic T-cell response as hosts in the radiation-genetic chimera model (**Fig. 4A**). As expected, tumor frequency was unaffected by nude host irradiation (Supplementary Fig. 2J, K). In this case, acceleration of tumor latency (Supplementary Fig. 2L) was lost between irradiated and sham Ncr nude hosts. However, the tumor growth rate in irradiated nude mice was still significantly increased compared to sham-irradiated nude mice (**Fig. 4B**; Supplementary Fig. 3E,F). Tumors from irradiated nude mice also showed more COX2 (**Fig. 4C**) and TGF β (**Fig. 4D**), and increased CD11b⁺ and CD11b⁺Gr1⁺ myeloid cells (**Fig. 4E,F**).

Tumor cell apoptosis significantly correlates with tumor infiltration of cytotoxic T cells in our prior study (20) but these cells are not mature and functional in athymic nude mice. Unexpectedly, apoptotic cells were decreased in tumors from irradiated hosts compared with tumors from sham hosts (**Fig. 4G**). Natural killer (NK) cells are reported to exhibit increased cytotoxic activity in immunodeficient mice as a compensation to dysfunction of T lymphocytes (30). Thus, we investigated whether activated NK cells marked by CD335 (NKp46) were correlated with tumor cell apoptosis. Consistent with increased tumor growth rate, NK cells were less abundant in tumors from irradiated hosts (**Fig. 4H**), supporting decreased immunosurveillance in the TME of tumors arising in irradiated hosts but raising the significance

of innate immunity in the process. Certain macrophage phenotypes are associated with tumor progression (31) and transcriptomic analysis of irradiated tissues indicated enrichment of a macrophage signature, which was also prominent in tumors arising in irradiated hosts (26,32).

Macrophages are recruited to the irradiated mammary gland and facilitate dysplastic morphogenesis in human cells.

Our initial hypothesis was that cytotoxic lymphocytes were key to the biology resulting in faster growth rate and iTME of tumors arising in irradiated mice, yet we found similar effect of radiation in immunodeficient mice. Hence, we posited that the establishment of an iTME implicated myeloid cells because they would be common to both immune competent and incompetent mice. Macrophages, as key mediators of tissue inflammatory response, may participate in early establishment of a pre-cancer niche that allows clonal expansion of initiated cells (8). Given this idea, we sought to localize mature macrophages marked by F4/80 adjacent to mammary epithelial ducts, which we reasoned could be involved in early carcinogenesis. Increased presence of F4/80⁺ macrophages were found proximal to *Trp53* null mammary outgrowth at 3 months post irradiation (1 Gy) compared to age-matched non-irradiated controls (**Fig. 5A**). Thus, macrophages typically described as pro-tumorigenic in advanced tumors (33) were more abundant in irradiated tissues well before cancer develops.

One of the earliest events in carcinogenesis is a disrupted morphogenesis, described *in situ* as dysplasia. To study the mechanisms by which macrophages may contribute to early events of carcinogenesis, we established 3D co-cultures of primary differentiated macrophages and irradiated non-malignant breast epithelial cells (MCF10A) embedded in Matrigel (**Fig. 5B**). Different subtypes of macrophages have distinct association with tissue homeostasis and carcinogenesis. Donor human peripheral blood monocytes (PBMC) were used to isolate CD14⁺ monocytes, which were polarized into classically activated (M1) and alternative activated (M2) macrophages as discussed in the Methods (Supplementary Fig. 4A,B). M1 and M2 were further activated by LPS and IFN γ (M1+) or IL-4 and TGF β (M2+) respectively. MCF10 cells were exposed to low dose of irradiation prior to addition of macrophages. Irradiated MCF10A that were co-cultured with activated M2 (M2+) formed significant larger (**Fig. 5C,D**) and less uniform acinar-like colonies (**Fig. 5E,F**) when cultured embedded in Matrigel.

Macrophages are known to secrete several inflammatory cytokines including IFN γ upon stimulation (34-40). IFN γ can release epithelial cell junctions during inflammatory conditions (41-43), which maybe an important factor in the aberrant morphogenesis phenotype. We confirmed that activated M2+ macrophages produce IFN γ by both mRNA and immunostaining (Supplementary Fig. 4C,D). To test whether IFN γ was mediating dysplastic morphogenesis, we treated co-cultures with IFN- γ neutralizing antibodies. IFN γ blockade in M2+ macrophage co-cultures restored MCF10A acinar morphogenesis (**Fig. 5C-F**).

Our prior work showed that TGF β activation induced by radiation can polarize and activate macrophages (26,32,44). These data show that activated macrophages in turn locally release epithelial junctions via IFN γ that promotes early dysplasia and aberrant morphogenesis. These data, together with the animal studies, suggest that irradiation elicited inflammation is key to the establishment of an iTME.

Aspirin treatment after irradiation abolishes iTME and rapid tumor growth

Prior radiation exposure of either humans or the genetic-chimera mouse model led to carcinomas exhibiting elevated pro-inflammatory factors, COX2 and TGF β . Moreover, our co-culture model indicated that macrophages cooperated with TGF β regulating tumorigenesis early events through another pro-inflammatory cytokine, IFN γ . To test whether modulating inflammation early in carcinogenesis affected the TME and aggressive cancer, we treated mice for 6-month with low dose aspirin (0.1 mg/ml in drinking water) immediately following irradiation and before any tumors are established (**Fig. 6A**). Aspirin is a commonly used anti-inflammation medicine that inactivates COX1 and COX2 (45) and has also been reported to reduce the production of IFN γ and TNF α by immune cells (46,47).

Consistent with carcinogenesis in the radiation-genetic chimera, neither tumor frequency nor latency was affected by radiation with or without aspirin (Supplementary Fig. 5A,B). Prior to tumor development, aspirin treatment prevented the radiation-induced accumulation of macrophages around *Trp53* null outgrowths (**Fig. 6B**; Supplementary Fig. 5C). The presence of F4/80⁺ macrophages was also reduced in tumors that subsequently formed in aspirin-treated irradiated hosts compared to tumors from untreated irradiated hosts (**Fig. 6C**; Supplementary 5D). Moreover, aspirin also decreased the presence of CD11b⁺/Gr1⁺ myeloid cells in tumors from the irradiated host (**Fig. 6D**; Supplementary Fig. 5E). Aspirin intervention also significantly decreased COX2 and TGF β intensity in tumors from irradiated hosts (**Fig. 6E,F**; Supplementary Fig. 5F).

Aspirin intervention post-radiation but prior to tumor development did not change tumor proliferation rate as indicated by Ki67⁺pan-cytokeratin⁺ tumor cells (Supplementary Fig. 6A). However, both CD3⁺ and cytotoxic CD8⁺ TIL were significantly increased in tumors from aspirin-treated irradiated host (**Fig. 6G**; Supplementary Fig. 6B). Concomitantly, proliferation of CD8⁺ T cells (Ki67⁺CD8⁺) was significantly increased in tumors from aspirin-treated irradiated hosts, indicating an active anti-tumor immunity similar to those tumors arising from sham-irradiated hosts (**Fig. 6H**; Supplementary Fig. 6C). Consistent with the increased CD8⁺ T cell activity, more apoptotic cells were present in tumors from aspirin treated, irradiated hosts compared to tumors from untreated irradiated hosts (**Fig. 6I**; Supplementary Fig. 6D). The growth rate of tumors arising in irradiated mice was significantly decreased by the aspirin intervention (**Fig. 6J**; Supplementary Fig. 7), consistent with an active cytotoxic immune surveillance that impedes tumor growth. These data support radiation-induced inflammation as a key mechanism that drives cancer to evolve towards an immunosuppressive, aggressive tumor.

Discussion

The risk of developing breast cancer at a young age (<50) is increased among women who received chest radiation for pediatric and young adult cancers to a level comparable to that of women at a comparable age who carry *BRCA1* germline mutations (1,2,6). Moreover RP-BC have features of more aggressive cancer (3-5). Our studies of a novel cohort of RP-BC and age-matched sporadic-BC revealed that RP-BC were characterized by a highly iTME with abundant TGF β , COX-2 and myeloid cells. Using stepwise evaluation of radiation effects on the epithelium, the host and the immune system in a murine mammary carcinogenesis model

recapitulated the iTME and revealed that radiation effects on innate immunity is key to iTME construction and aggressive growth. When the transplant epithelium was irradiated, tumor incidence and growth rate increased, latency decreased, and these tumors exhibited iTME similar to RP-BC. However, when mice were irradiated prior to mammary transplantation, host irradiation still elicited the establishment of the iTME and increased tumor growth rate. Our initial hypothesis was that cytotoxic lymphocytes were key to the biology of fast growth and iTME of tumors arising in irradiated mice, yet we found similar effects of radiation in immune compromised nude mice: host irradiation prior to transplantation in nude mice did not eliminate differential growth rate or iTME. Hence, we posited that the establishment of an iTME in nude mice implicated myeloid cells because they are common to both immune competent and incompetent mice. A combination of *in situ* analysis and human cell co-culture experiments revealed a specific pro-inflammatory, IFN γ mediated mechanism by which activated macrophages promote dysplasia, an early event in carcinogenesis. This conclusion was supported by anti-inflammatory treatment with aspirin after irradiation, which eliminated iTME features and decreased tumor growth rate.

The concept that the establishment of an iTME follows radiation exposure adds credence to the use of anti-inflammatory agents in breast cancer prevention. Aspirin inactivates COX1 and COX2 (45). COX2 is important in all stages of tumor progression (24), and may be a critical factor in allowing cancer cells to escape host immune defenses by modulation of cytokine production, dysfunction of dendritic cells, myeloid derived suppressor cells generation (48) and suppression of lymphocyte proliferation associated with immunosuppression and tumorigenesis (49). Consistent with this, COX2 was significantly upregulated in the TME of tumors arising from irradiated hosts, but when treated with aspirin, COX2 expression significantly decreased. High TIL are a favorable prognostic factor in TNBC (22,50)]. Consistent with our findings, COX2 inhibition in mice accelerates accumulation of cytotoxic T cells within tumors that have slow tumor growth (51). An ongoing clinical trial using aspirin as an adjuvant therapy for breast cancer (NCT02927249) may reveal similar benefit.

Our studies extend the finding by Horst et al. that the spectrum of cancers in RP-BC is distinct from that of age-matched sporadic-BC. RP-BC is reported to be more aggressive in several studies (3-5), but not all (7). Importantly, cancer survivors also have a poor prognosis because of other health-related causes, including other subsequent malignant neoplasms and cardiovascular or pulmonary disease (7). Considerable clinical evidence now associates TIL with cancer prognosis (22,50); thus, the absence of TIL in RP-BC is consistent with the previous clinical observations. Both RP-BC and mammary carcinomas arising in irradiated mice were enriched in TGF β compared to cancers arising in unirradiated humans or mice. TGF β is classically considered a tumor suppressor, largely due to its function in the control of proliferation in normal epithelial cells, but it is clear that it also promotes cancer by regulating the characteristics and composition of the TME, including suppressing adaptive immunity and promoting pro-tumorigenic myeloid cells (52). Our previous studies showed that radiation induced TGF β activation regulates tissue (e.g. extracellular matrix remodeling), stromal (e.g. recruitment and polarization of immune cells) and cellular (e.g. DNA damage response) radiation effects (53). The prominence of TGF β involvement in radiation responses is


provocative because it also orchestrates multiple levels of inflammation, angiogenesis and immune function that are associated with aggressive cancer (54).

Low doses of ionizing radiation do not elicit substantial tissue damage or gross inflammation but rather shift the activation state of tissue resident cells, like macrophage polarization, which are a class of radiation effects that are called non-targeted (55). Classic M1 polarization is elicited by Th1 cytokines; the resulting phenotype is thought to be important in cell phagocytosis and is anti-tumorigenic. The M2 phenotype is elicited by Th2 cytokines and is associated with tumor promotion (56). The high activity of TGF β in the TME likely promotes monocyte recruitment (57) and regulates macrophage polarization, skewing differentiation toward an M2 suppressive phenotype (58). TGF β promotes the recruitment of bone marrow derived cells and is associated with breast cancer prognosis (59,60). Here we found macrophages were increased in mammary tissues shortly after radiation exposure and were elevated in tumors arising in irradiated hosts.

Macrophages play a significant role in most solid malignancies. Macrophage abundance is associated with increased micro-vessel density and reduced patient survival in breast cancer (61-63). In fact, macrophages present within tumors are defined as tumor-associated macrophages to denote a specific phenotype that is associated with the production of several proangiogenic factors, cytokines, and metabolites that suppress anti-tumor immune responses and promote tumor growth by maintaining pro-tumorigenic inflammation (64). The etiology of aggressive TNBC, which is also more common in *BRCA1* germline carriers and African-American women (65), is still poorly understood, but the observation that RP-BC are enriched in TNBC could provide a new perspective on their genesis or biomarkers of TNBC risk

These experimental studies have several limitations that affect generalization of our conclusions. First, the high-dose fractionated exposures that are used to treat HL patients were not replicated in our experiments. The doses used for the studies in mice ranged from 0.1 to 1 Gy, which are far below that delivered during radiotherapy. Neither tumor incidence nor composition were dose dependent in the genetic mammary chimera model, whereas risk of secondary breast cancer increases with radiation dose (66). Thus, additional mechanisms may arise at higher doses or with fractionated exposure, which are key factors to explore in further experiments. Nonetheless, low-dose, whole-body irradiation of mice recapitulated the iTME evident in RP-BC. Second, the *Trp53* null mammary chimera is a single genetic mouse model, albeit one that generates diverse carcinomas. Third, although radiation is the strongest treatment-associated risk factor for breast cancer, risk is also increased by exposure to chemotherapy (particularly anthracyclines) and can be further altered by gonadal hormone exposure (67). It is thought that the protective effect of alkylating chemotherapy decreases breast cancer risk among female HL survivors due to premature menopause (68).

The annual dose of the American public from use of ionizing radiation in diagnostic and therapeutic medical applications has doubled over the last 20 years (69). As Americans live longer, the cumulative burden of medical radiation exposure will contribute significantly to cancer incidence. Here, our irradiated mouse experiments show that non-mutational mechanisms that alter signals and cells associated with innate immunity alter the course of carcinogenesis toward more aggressive disease. The identification of these non-mutational, so-



called non-targeted radiation effects are important for predicting radiation risks, particularly in cancer survivors who have life-long morbidity that might be amenable to intervention.



Acknowledgements

The authors would like to thank Dr. Jade Moore for helpful suggestions, Dr. Oliver Reiners for image analysis suggestions, and Dr. Xiao Lu Li, Mr. Dixon F Hoffelt, Mr. Trevor Jones and Ms. Hui Zhang for technical support. The authors also thank Dr. Ann Lazar and Dr. Jian-Hua Mao for advice on biostatistics and data analysis.

This research was supported by NASA Specialized Center for Research in Radiation Health Effects, NNX09AM52G, and NNX13AF06G at New York University School of Medicine and NIH R01CA190980 at UCSF to M.H. Barcellos-Hoff.

References

1. Henderson TO, Amsterdam A, Bhatia S, Hudson MM, Meadows AT, Neglia JP, *et al.* Systematic review: surveillance for breast cancer in women treated with chest radiation for childhood, adolescent, or young adult cancer. *Ann Intern Med* **2010** 152(7):444-55 doi 20368650.
2. Bhatia S, Robison LL, Oberlin O, Greenberg M, Bunin G, Fossati-Bellani F, *et al.* Breast cancer and other second neoplasms after childhood Hodgkin's disease. *N Engl J Med* **1996**;334(12):745-51.
3. Castiglioni F, Terenziani M, Carcangiu ML, Miliano R, Aiello P, Bertola L, *et al.* Radiation effects on development of HER2-positive breast carcinomas. *Clin Cancer Res* **2007**;13(1):46-51 doi 10.1158/1078-0432.ccr-06-1490.
4. Broeks A, Braaf LM, Wessels LF, van de Vijver M, De Bruin ML, Stovall M, *et al.* Radiation-associated breast tumors display a distinct gene expression profile. *Int J Radiat Oncol Biol Phys* **2010**;76(2):540-7 doi 10.1016/j.ijrobp.2009.09.004.
5. Horst KC, Hancock SL, Ognibene G, Chen C, Advani RH, Rosenberg SA, *et al.* Histologic subtypes of breast cancer following radiotherapy for Hodgkin lymphoma. *Annals of Oncology* **2014**;25(4):848-51 doi 10.1093/annonc/mdu017.
6. Moskowitz CS, Chou JF, Wolden SL, Bernstein JL, Malhotra J, Novetsky Friedman D, *et al.* Breast cancer after chest radiation therapy for childhood cancer. *Journal of clinical oncology : official journal of the American Society of Clinical Oncology* **2014**;32(21):2217-23 doi 10.1200/jco.2013.54.4601.
7. Moskowitz CS, Chou JF, Neglia JP, Partridge AH, Howell RM, Diller LR, *et al.* Mortality After Breast Cancer Among Survivors of Childhood Cancer: A Report From the Childhood Cancer Survivor Study. *Journal of clinical oncology : official journal of the American Society of Clinical Oncology* **2019**;37(24):2120-30 doi 10.1200/jco.18.02219.
8. Barcellos-Hoff MH, Lyden D, Wang TC. The evolution of the cancer niche during multistage carcinogenesis. *Nat Rev Cancer* **2013**;13(7):511-8 doi 10.1038/nrc3536.
9. Barcellos-Hoff MH, Park C, Wright EG. Radiation and the microenvironment - tumorigenesis and therapy. *Nat Rev Cancer* **2005**;5(11):867-75.
10. Little MP, Filipe JAN, Prise KM, Folkard M, Belyakov OV. A model for radiation-induced bystander effects, with allowance for spatial position and the effects of cell turnover. *Journal of theoretical biology* **2005**;232(3):329-38.
11. Barcellos-Hoff MH. Radiation-induced transforming growth factor β and subsequent extracellular matrix reorganization in murine mammary gland. *Cancer research* **1993**;53:3880-6.
12. Tang C, Wang X, Soh H, Seyedin S, Cortez MA, Krishnan S, *et al.* Combining radiation and immunotherapy: a new systemic therapy for solid tumors? *Cancer immunology research* **2014**;2(9):831-8 doi 10.1158/2326-6066.cir-14-0069.
13. Grivennikov SI, Greten FR, Karin M. Immunity, Inflammation, and Cancer. *Cell* **2010**;140(6):883-99 doi 10.1016/j.cell.2010.01.025.
14. Dunn GP, Bruce AT, Ikeda H, Old LJ, Schreiber RD. Cancer immunoediting: from immunosurveillance to tumor escape. *Nature Immunol* **2002**;3:991-8.
15. Chen DS, Mellman I. Elements of cancer immunity and the cancer-immune set point. *Nature* **2017**;541(7637):321-30 doi 10.1038/nature21349.
16. Stanton SE, Adams S, Disis ML. Variation in the Incidence and Magnitude of Tumor-Infiltrating Lymphocytes in Breast Cancer Subtypes: A Systematic Review. *JAMA oncology* **2016**;2(10):1354-60 doi 10.1001/jamaoncol.2016.1061.

17. Hegde PS, Karanikas V, Evers S. The Where, the When, and the How of Immune Monitoring for Cancer Immunotherapies in the Era of Checkpoint Inhibition. *Clin Cancer Res* **2016**;22(8):1865-74 doi 10.1158/1078-0432.ccr-15-1507.
18. Thorsson V, Gibbs DL, Brown SD, Wolf D, Bortone DS, Ou Yang T-H, *et al.* The Immune Landscape of Cancer. *Immunity* **2018**;48(4):812-30.e14 doi 10.1016/j.immuni.2018.03.023.
19. Swartz MA, Iida N, Roberts EW, Sangaletti S, Wong MH, Yull FE, *et al.* Tumor microenvironment complexity: emerging roles in cancer therapy. *Cancer research* **2012**;72(10):2473-80 doi 10.1158/0008-5472.CAN-12-0122.
20. Omene C, Ma L, Moore J, Ouyang H, Illa-Bochaca I, Chou W, *et al.* Aggressive Mammary Cancers Lacking Lymphocytic Infiltration Arise in Irradiated Mice and Can Be Prevented by Dietary Intervention. *Cancer immunology research* **2020**;8(2):217-29 doi 10.1158/2326-6066.cir-19-0253.
21. Gonzalez-Junca A, Driscoll KE, Pellicciotta I, Du S, Lo CH, Roy R, *et al.* Autocrine TGFbeta Is a Survival Factor for Monocytes and Drives Immunosuppressive Lineage Commitment. *Cancer immunology research* **2019**;7(2):306-20 doi 10.1158/2326-6066.cir-18-0310.
22. Loi S, Drubay D, Adams S, Pruneri G, Francis PA, Lacroix-Triki M, *et al.* Tumor-Infiltrating Lymphocytes and Prognosis: A Pooled Individual Patient Analysis of Early-Stage Triple-Negative Breast Cancers. *Journal of clinical oncology : official journal of the American Society of Clinical Oncology* **2019**;37(7):559-69 doi 10.1200/JCO.18.01010.
23. Hu M, Peluffo G, Chen H, Gelman R, Schnitt S, Polyak K. Role of COX-2 in epithelial-stromal cell interactions and progression of ductal carcinoma in situ of the breast. *Proc Natl Acad Sci (USA)* **2009**;106(9):3372-7 doi 10.1073/pnas.0813306106.
24. Choy H, Milas L. Enhancing Radiotherapy With Cyclooxygenase-2 Enzyme Inhibitors: A Rational Advance? *JNCI: Journal of the National Cancer Institute* **2003**;95(19):1440-52 doi 10.1093/jnci/djg058.
25. Elliott LA, Doherty GA, Sheahan K, Ryan EJ. Human Tumor-Infiltrating Myeloid Cells: Phenotypic and Functional Diversity. *Frontiers in immunology* **2017**;8:86 doi 10.3389/fimmu.2017.00086.
26. Nguyen DH, Oketch-Rabah HA, Illa-Bochaca I, Geyer FC, Reis-Filho JS, Mao JH, *et al.* Radiation Acts on the Microenvironment to Affect Breast Carcinogenesis by Distinct Mechanisms that Decrease Cancer Latency and Affect Tumor Type. *Cancer Cell* **2011**;19(5):640-51 doi 10.1016/j.ccr.2011.03.011.
27. Mariathasan S, Turley SJ, Nickles D, Castiglioni A, Yuen K, Wang Y, *et al.* TGFbeta attenuates tumour response to PD-L1 blockade by contributing to exclusion of T cells. *Nature* **2018**;554(7693):544-8 doi 10.1038/nature25501.
28. Allred DC, Wu Y, Mao S, Nagtegaal ID, Lee S, Perou CM, *et al.* Ductal Carcinoma In situ and the Emergence of Diversity during Breast Cancer Evolution. *Clin Cancer Res* **2008**;14(2):370-8 doi 10.1158/1078-0432.ccr-07-1127.
29. Illa-Bochaca I, Ouyang H, Tang J, Sebastiano C, Mao J-H, Costes SV, *et al.* Densely Ionizing Radiation Acts via the Microenvironment to Promote Aggressive Trp53 Null Mammary Carcinomas. *Cancer research* **2014**;74(23):7137-48 doi 10.1158/0008-5472.CAN-14-1212.
30. Budzynski W, Radzikowski C. Cytotoxic Cs in Immunodeficient Athymic Mice. *Immunopharmacology and Immunotoxicology* **1994**;16(3):319-46 doi 10.3109/08923979409007097.
31. Mukhtar RA, Nseyo O, Campbell MJ, Esserman LJ. Tumor-associated macrophages in breast cancer as potential biomarkers for new treatments and diagnostics. *Expert Review of Molecular Diagnostics* **2010**;11(1):91-100 doi doi:10.1586/erm.10.97.

32. Nguyen DH, Fredlund E, Zhao W, Perou CM, Balmain A, Mao J-H, *et al.* Murine Microenvironment Metaprofiles Associate with Human Cancer Etiology and Intrinsic Subtypes. *Clin Cancer Research* **2013**;19(6):1353-62 doi 10.1158/1078-0432.ccr-12-3554.
33. Gyorki DE, Lindeman GJ. Macrophages, more than just scavengers: their role in breast development and cancer. *ANZ J Surg* **2008**;78:432-6.
34. Darwich L, Coma G, Pena R, Bellido R, Blanco EJ, Este JA, *et al.* Secretion of interferon-gamma by human macrophages demonstrated at the single-cell level after costimulation with interleukin (IL)-12 plus IL-18. *Immunology* **2009**;126(3):386-93 doi 10.1111/j.1365-2567.2008.02905.x.
35. Munder M, Mallo M, Eichmann K, Modolell M. Murine macrophages secrete interferon gamma upon combined stimulation with interleukin (IL)-12 and IL-18: A novel pathway of autocrine macrophage activation. *Journal of Experimental Medicine* **1998**;187(12):2103-8 doi DOI 10.1084/jem.187.12.2103.
36. Puddu P, Fantuzzi L, Borghi P, Varano B, Rainaldi G, Guillemard E, *et al.* IL-12 induces IFN-gamma expression and secretion in mouse peritoneal macrophages. *Journal of immunology* **1997**;159(7):3490-7.
37. Di Marzio P, Puddu P, Conti L, Belardelli F, Gessani S. Interferon gamma upregulates its own gene expression in mouse peritoneal macrophages. *The Journal of experimental medicine* **1994**;179(5):1731-6.
38. Gessani S, Belardelli F. IFN-gamma expression in macrophages and its possible biological significance. *Cytokine & growth factor reviews* **1998**;9(2):117-23.
39. Fultz MJ, Barber SA, Dieffenbach CW, Vogel SN. Induction of IFN-gamma in macrophages by lipopolysaccharide. *International immunology* **1993**;5(11):1383-92.
40. Puddu P, Carollo M, Pietraforte I, Spadaro F, Tombesi M, Ramoni C, *et al.* IL-2 induces expression and secretion of IFN-gamma in murine peritoneal macrophages. *Journal of leukocyte biology* **2005**;78(3):686-95 doi 10.1189/jlb.0105035.
41. Kudryavets YI, Bezdenezhnykh NO, Lykhova OO, Semesiuk NI, Vorontsova AL. The role of interferon as a modifier of epithelial-mesenchymal transition in tumor cells. *Experimental oncology* **2011**;33(3):178-81.
42. Smyth D, Leung G, Fernando M, McKay DM. Reduced surface expression of epithelial E-cadherin evoked by interferon-gamma is Fyn kinase-dependent. *PloS one* **2012**;7(6):e38441 doi 10.1371/journal.pone.0038441.
43. Nava P, Koch S, Laukoetter MG, Lee WY, Kolegraff K, Capaldo CT, *et al.* Interferon-gamma Regulates Intestinal Epithelial Homeostasis through Converging beta-Catenin Signaling Pathways. *Immunity* **2010**;32(3):392-402 doi 10.1016/j.immuni.2010.03.001.
44. Tang J, Fernandez-Garcia I, Vijayakumar S, Martinez-Ruiz H, Illa-Bochaca I, Nguyen DH, *et al.* Irradiation of juvenile, but not adult, mammary gland increases stem cell self-renewal and estrogen receptor negative tumors. *Stem Cells* **2013**;32(3):649-61 doi 10.1002/stem.1533.
45. Lohaus F, Linge A, Tinhofer I, Budach V, Gkika E, Stuschke M, *et al.* HPV16 DNA status is a strong prognosticator of loco-regional control after postoperative radiochemotherapy of locally advanced oropharyngeal carcinoma: Results from a multicentre explorative study of the German Cancer Consortium Radiation Oncology Group (DKTK-ROG). *Radiotherapy and Oncology* **2014**;113(3):317-23 doi 10.1016/j.radonc.2014.11.011.
46. Mateo J, Carreira S, Sandhu S, Miranda S, Mossop H, Perez-Lopez R, *et al.* DNA-Repair Defects and Olaparib in Metastatic Prostate Cancer. *N Engl J Med* **2015**;373(18):1697-708 doi 10.1056/NEJMoa1506859.
47. Noordermeer SM, Adam S, Setiাপutra D, Barazas M, Pettitt SJ, Ling AK, *et al.* The shieldin complex mediates 53BP1-dependent DNA repair. *Nature* **2018**;560(7716):117-21 doi 10.1038/s41586-018-0340-7.

48. Obermajer N, Muthuswamy R, Lesnock J, Edwards RP, Kalinski P. Positive feedback between PGE2 and COX2 redirects the differentiation of human dendritic cells toward stable myeloid-derived suppressor cells. *Blood* **2011**;118(20):5498-505 doi 10.1182/blood-2011-07-365825.
49. Hashemi Goradel N, Najafi M, Salehi E, Farhood B, Mortezaee K. Cyclooxygenase-2 in cancer: A review. *Journal of cellular physiology* **2019**;234(5):5683-99 doi 10.1002/jcp.27411.
50. Denkert C, von Minckwitz G, Darb-Esfahani S, Lederer B, Heppner BI, Weber KE, *et al.* Tumour-infiltrating lymphocytes and prognosis in different subtypes of breast cancer: a pooled analysis of 3771 patients treated with neoadjuvant therapy. *The Lancet Oncology* **2018**;19(1):40-50 doi 10.1016/s1470-2045(17)30904-x.
51. DeLong P, Tanaka T, Kruklitis R, Henry AC, Kapoor V, Kaiser LR, *et al.* Use of cyclooxygenase-2 inhibition to enhance the efficacy of immunotherapy. *Cancer research* **2003**;63(22):7845-52.
52. Bierie B, Moses HL. Tumour microenvironment: TGFbeta: the molecular Jekyll and Hyde of cancer. *Nat Rev Cancer* **2006**;6(7):506-20.
53. Andarawewa KL, Kirshner J, Mott JD, Barcellos-Hoff MH. TGFβ: Roles in DNA damage responses. In: Jakowlew S, editor. *Transforming Growth Factor-Beta in Cancer Therapy, Volume II Cancer Treatment and Therapy. Volume II, Cancer Drug Discovery and Development.* Totowa: Humana Press; 2007. p 321-34.
54. Barcellos-Hoff MH, Akhurst RJ. Transforming growth factor-beta in breast cancer: too much, too late. *Breast cancer research and treatment* **2010**;11(1):202-08.
55. Barcellos-Hoff MH. How do tissues respond to damage at the cellular level? The role of cytokines in irradiated tissues. *Radiation research* **1998**;150(5):S109-S20.
56. Qian BZ, Pollard JW. Macrophage diversity enhances tumor progression and metastasis. *Cell* **2010**;141(1):39-51 doi 10.1016/j.cell.2010.03.014.
57. Wahl SM, Hunt DA, Wakefield LM, McCartney-Francis N, Wahl M, Roberts AB, *et al.* Transforming growth-factor beta (TGF-beta) induces monocyte chemotaxis and growth factor production. *Proc Natl Acad Sci USA* **1987**;84:5788-91.
58. Yang WC, Ma G, Chen SH, Pan PY. Polarization and reprogramming of myeloid-derived suppressor cells. *Journal of molecular cell biology* **2013**;5(3):207-9 doi 10.1093/jmcb/mjt009.
59. Bierie B, Stover DG, Abel TW, Chytil A, Gorska AE, Aakre M, *et al.* Transforming Growth Factor-β Regulates Mammary Carcinoma Cell Survival and Interaction with the Adjacent Microenvironment. *Cancer research* **2008**;68(6):1809-19 doi 10.1158/0008-5472.CAN-07-5597.
60. Bierie B, Chung CH, Stover DG, Cheng N, Parker J, Chytil A, *et al.* Abrogation of TGF-β signaling enhances chemokine production and correlates with prognosis in human breast cancer. *J Clin Invest* **2009**;119(1571-1582).
61. Leek RD, Lewis CE, Whitehouse R, Greenall M, Clarke J, Harris AL. Association of Macrophage Infiltration with Angiogenesis and Prognosis in Invasive Breast Carcinoma. *Cancer research* **1996**;56(20):4625-9.
62. Coffelt SB, Tal AO, Scholz A, De Palma M, Patel S, Urbich C, *et al.* Angiopoietin-2 regulates gene expression in TIE2-expressing monocytes and augments their inherent proangiogenic functions. *Cancer research* **2010**;70(13):5270-80.
63. Morita Y, Zhang R, Leslie M, Adhikari S, Hasan N, Chervoneva I, *et al.* Pathologic evaluation of tumor-associated macrophage density and vessel inflammation in invasive breast carcinomas. *Oncology letters* **2017**;14(2):2111-8 doi 10.3892/ol.2017.6466.
64. Noy R, Pollard JW. Tumor-associated macrophages: from mechanisms to therapy. *Immunity* **2014**;41(1):49-61 doi 10.1016/j.immuni.2014.06.010.
65. Schneider BP, Winer EP, Foulkes WD, Garber J, Perou CM, Richardson A, *et al.* Triple-negative breast cancer: risk factors to potential targets. *Clin Cancer Res* **2008**;14(24):8010-8 doi 10.1158/1078-0432.CCR-08-1208.

66. Van Leeuwen FE, Klokman WJ, Stovall M, Dahler EC, van't Veer MB, Noordijk EM, *et al.* Roles of radiation dose, chemotherapy, and hormonal factors in breast cancer following Hodgkin's disease. *J Natl Cancer Inst* **2003**;95(13):971-80.
67. Chao C, Bhatia S, Xu L, Cannavale KL, Wong FL, Huang P-YS, *et al.* Incidence, Risk Factors, and Mortality Associated With Second Malignant Neoplasms Among Survivors of Adolescent and Young Adult CancerSecond Malignant Neoplasms Among Survivors of Adolescent and Young Adult CancerSecond Malignant Neoplasms Among Survivors of Adolescent and Young Adult Cancer. *JAMA Network Open* **2019**;2(6):e195536-e doi 10.1001/jamanetworkopen.2019.5536.
68. Travis LB, Hill DA, Dores GM, Gospodarowicz M, van Leeuwen FE, Holowaty E, *et al.* Breast cancer following radiotherapy and chemotherapy among young women with Hodgkin disease. *Jama* **2003**;290(4):465-75.
69. UNSCEAR. Sources and effects of ionizing radiation New York: United Nations; 2006.

Figure Legends

Fig. 1 The TME of RP-BC is more immunosuppressive than that of sporadic-BC. A. Three infiltration patterns of lymphocytes are shown in representative images of human breast cancer sections stained with cytotoxic T cell marker CD8 (green) and DAPI (blue). Yellow scale bar=50 μm . White scale bar=1 mm. Tumors were classified as inflamed (orange), excluded (purple) or desert (grey) as described in Methods. The proportion of tumor types are shown as pie charts for sporadic-BC (n=43) and RP-BC group (n=21). **B-G.** Multiplex immunostaining of inflammatory factors and immune cell markers showed that RP-BC exhibit higher COX2 (**B**) and TGF β (**D**) compared with sporadic-BC. The RP-BC was more immunosuppressive abundant with (**C**) PD-L1⁺ and (**E**) CD11b⁺ cells. In contrast, sporadic-BC contained more CD4⁺ (**F**) and CD8⁺ lymphocytes (**G**). Sporadic-BC, n=43; RP-BC, n=22. Data shown were the means with SEM; *, p<0.05; ***, p<0.001; ****, p<0.0001 by Mann Whitney test.


Fig. 2 Cancer arising in the irradiated genetic chimera model recapitulate iTME of RP-BC. A. Genetic-chimera experimental scheme. BALB/c wild type mice were cleared and transplanted with *Trp53* null fragments at 3-week old, aged to 10-week old and irradiated. Mice were monitored for 500 days for tumorigenesis. **B.** Tumor growth rate fitted to an exponential curve and averaged over 30 days for each treatment group. Sham, n=17; IR, n=38. **, p<0.01 *F*-test. **C and D.** The mean intensity of COX2 and TGF β of tumors from IR mice (n=23) were higher than tumors from sham group (n=15). The frequency of CD11b⁺ (**E**, sham, n=15; IR, n=15) and Gr1⁺CD11b⁺ myeloid cells (**F**, sham, n=6; IR, n=11) was increased in tumors from IR mice. The frequency of CD3⁺ T lymphocytes (**G**, sham, n=6; IR, n=11) and CD8⁺ cytotoxic T cells (**H**, sham, n=6; IR, n=11) was decreased in in tumors from IR mice. **I.** Apoptosis marked by cleaved-Caspase3 was reduced in tumors arising in IR mice (n=7) compared to tumors in sham mice (n=7). Data shown in **C** to **I** were the means with SEM; *, p<0.05; **, p<0.01; ***, p<0.001; Mann-Whitney test.

Fig. 3 Radiation induced tumor immune features are mainly regulated by radiation effects on the host. A. Radiation-genetic chimera experimental scheme. BALB/c wild type mice were cleared fat-pad at 3-week old, aged to 10-week old, irradiated whole body and transplanted with *Trp53* null mammary fragments 3 days later. Mice were monitored for 500 days for tumorigenesis. **B.** Tumor growth rate fitted to an exponential curve and averaged over 30 days for each treatment group. Sham, n=22; IR, n=12. ****, p<0.0001. *F*-test. **C-D.** Tumors from IR group (n=9) showed a higher level of COX2 and TGF β intensity than tumors from sham group (n=17). Immunofluorescence staining showed CD11b⁺ (**E**, sham, n=8; IR, n=8) and Gr1⁺CD11b⁺ myeloid cells (**F**, sham, n=5; IR, n=6) were more infiltrated in tumors from IR group, while CD3⁺ T cells (**G**, sham, n=5; IR, n=6) and CD8⁺ cytotoxic T cells (**H**, sham, n=8; IR, n=8) were more infiltrated in tumors from sham group. **I.** Cell apoptosis marked by cleaved-Caspase3⁺ cells per HPF was reduced in tumors arising in IR group (n=10) than tumors in sham group (n=10). Data shown in **C** to **I** are the means with SEM; *, p<0.05; **, p<0.01; Mann-Whitney test.

Fig. 4 An iTME is established in the absence of cytotoxic T cells. **A.** Immuno-incompetent radiation-genetic chimera experimental scheme. Ncr nude mice were cleared at 4-week old, aged to 10-week old, irradiated whole body and transplanted with *Trp53* null mammary fragments 3 days later. Mice were monitored for 500 days for tumorigenesis. **B.** Tumor growth rate fitted to an exponential curve and averaged over 30 days for each treatment group. Sham, n=14; IR, n=13. **, p<0.01, F-test. The mean intensity of COX2 (**C**) and TGFβ (**D**) for tumor arising in IR mice (n=10) was increased compared to tumors from sham mice (n=9 for COX2; n=10 for TGFβ). Immunofluorescence staining showed tumors from IR group had more abundant CD11b⁺ (**E**, sham, n=10; IR, n=10) and Gr1⁺CD11b⁺ myeloid cells (**F**, sham, n=10; IR, n=10). While, apoptotic cells marked by cleaved-Caspase3 (**G**, sham, n=5; IR, n=6) and CD335⁺ NK cells (**H**, sham, n=11; IR, n=11) was less abundant in tumors arising in IR group. Data shown in **C** to **H** are the means with SEM; *, p<0.05; **, p<0.01; Mann-Whitney test.

Fig. 5 Macrophages are recruited to the irradiated mammary gland and facilitate dysplastic morphogenesis in human cells. **A.** Immunostaining of F4/80⁺ macrophages in *Trp53* null mammary outgrowths of the radiation-genetic chimera were 3 months after transplantation. Left, representative images of F4/80⁺ (brown) cells in mammary outgrowths from sham and IR mice. Yellow scale bar=20 μm. Black scale bar=200 μm. Red arrow indicates the regions shown in high-power. Right, quantification of F4/80⁺ cells, mean with SEM. Sham, n=6; IR, n=12. **, p<0.01; unpaired t-test. **B.** Schematic representation of the experimental design. MCF10A cells were seeded at high density and irradiated as confluent cultures, treated with TGFβ and co-cultured with activated macrophages in the presence or absence of IFNγ neutralizing antibody for 7 days. CD45⁻ negative epithelial cells were sorted from the co-cultures and reseeded on Matrigel for 15 days. **C.** Representative images of the MCF10A morphogenesis as a function of irradiation and co-culture with macrophages. MCF10ADCIS.com is shown as a positive control for dysplasia (DCIS). Black scale bar=100 μm. Morphology was quantified from bright field images as mean acini area (**D**) and perimeter (**E**). Data from 3 independent experiments are shown as mean with SEM. *, p<0.05; **, p<0.01; One way-ANOVA. **F.** The shape factor for each acinus from 3 independent experiments is shown as violin plot with median. *, p<0.05; **, p<0.01; Kruskal-Wallis test.

Fig. 6 Aspirin treatment after irradiation abolishes iTME and rapid tumor growth. **A.** Aspirin treated radiation-genetic experimental scheme. BALB/c wild type mice were cleared fat-pad at 3-week old, aged to 10-week old, irradiated whole body and transplanted with *Trp53* null mammary fragments 3 days later. Aspirin was given in drinking water for 6 months after whole body irradiation and monitored for 500 days for tumorigenesis. **B.** IHC quantification of F4/80⁺ cells in mammary outgrowths from sham (n=7), aspirin (n=4), IR (n=8) and IR+aspirin (n=6) treated mice. **C.** IHC quantification of F4/80⁺ cells in mammary tumors from sham (n=18), aspirin (n=17), IR (n=14), IR+aspirin (n=15) treated mice. **D.** Immunofluorescence staining quantifications of Gr1⁺CD11b⁺ myeloid cells. Sham, n=18; aspirin, n=17; IR, n=13; IR+aspirin, n=16. **E.** Aspirin decreased the mean intensity of COX2 immunofluorescence staining. Sham, n=18; aspirin, n=16; IR, n=13; IR+aspirin, n=16. **F.** Aspirin decreased TGFβ mean intensity in



immunofluorescence staining. Sham, n=17; aspirin, n=17; IR, n=12; IR+aspirin, n=13. **G.** Immunofluorescence staining quantification of CD8⁺ T cells. Sham, n=18; aspirin, n=18; IR, n=14; IR+aspirin, n=16. **H.** Immunofluorescence staining quantification of proliferating cytotoxic T cells marked as Ki67 and CD8 double positive cells. Sham, n=18; aspirin, n=18; IR, n=14; IR+aspirin, n=16. **I.** Immunofluorescence staining quantification of apoptotic cells marked by cleaved-Caspase3. Sham, n=13; aspirin, n=8; IR, n=9; IR+aspirin, n=9. Data shown in **B-I** are the means with SEM; *, p<0.05; **, p<0.01; ***, p<0.001; One-way ANOVA. **J.** Tumor growth rate fitted to an exponential curve and averaged over 30 days for each treatment group. Sham, n=15, black; aspirin, n=10, purple; IR, n=12, green; IR+aspirin, blue, n=11. **, p<0.01. ***, p<0.001. One-way ANOVA.

Figure 1

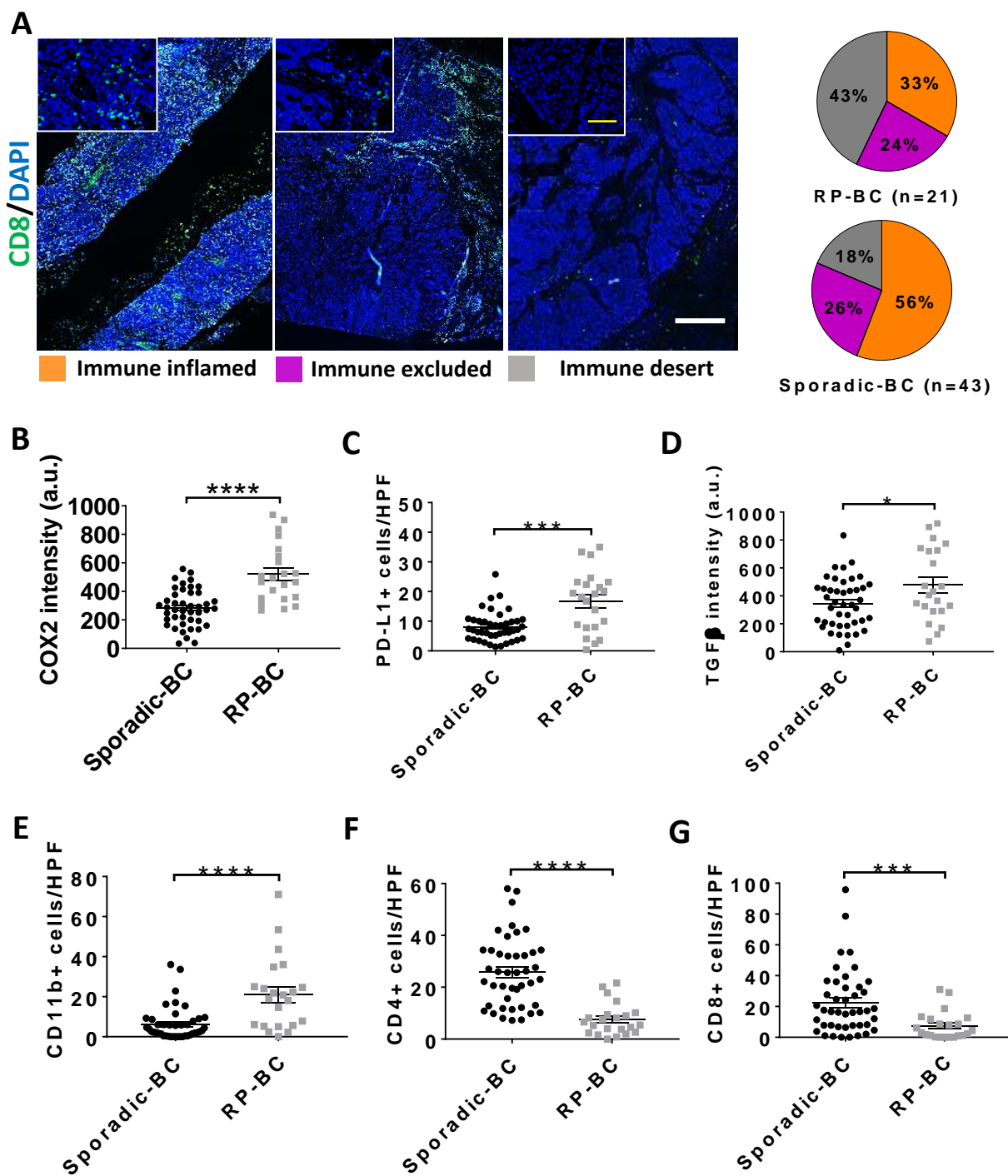


Figure 2

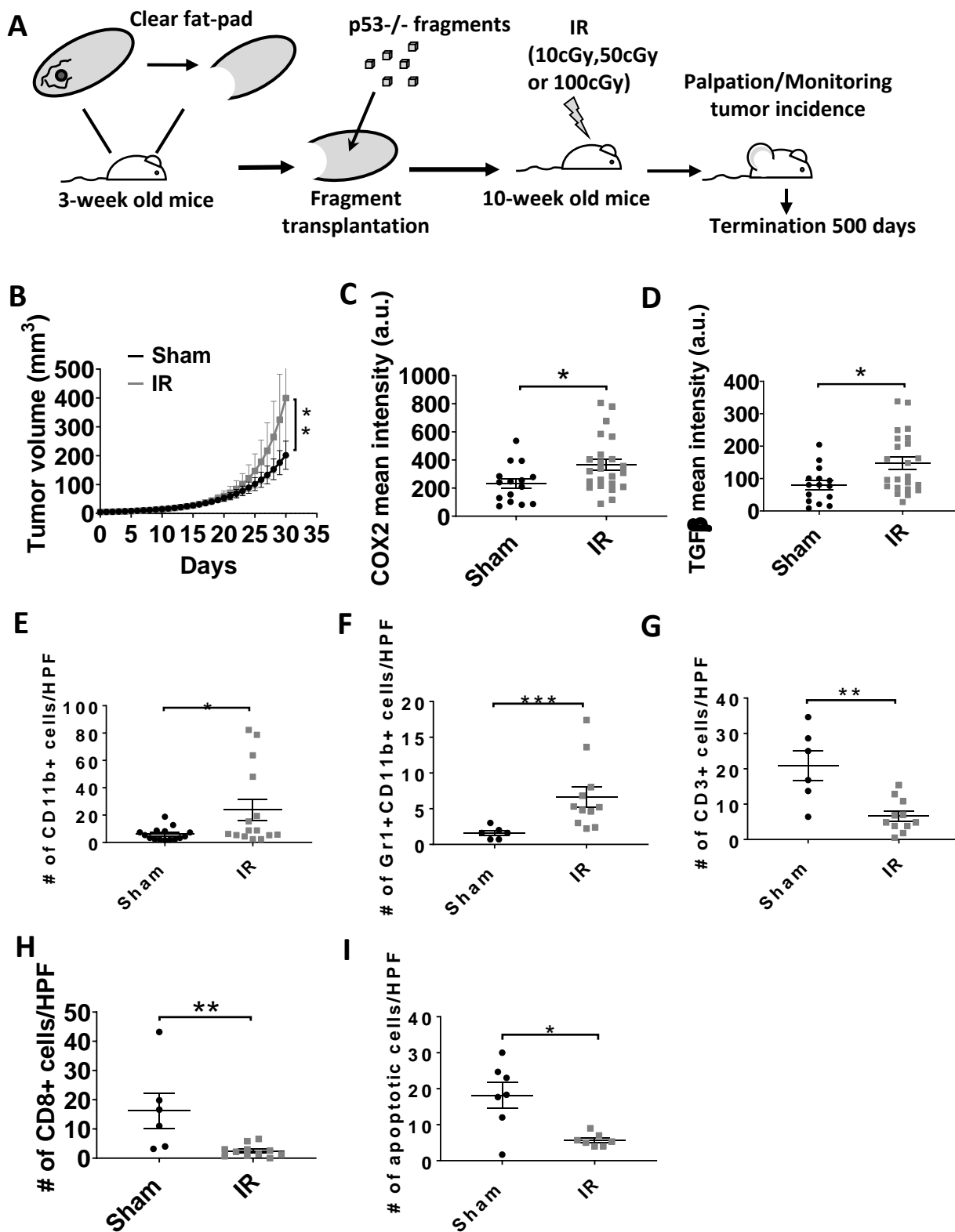


Figure 3

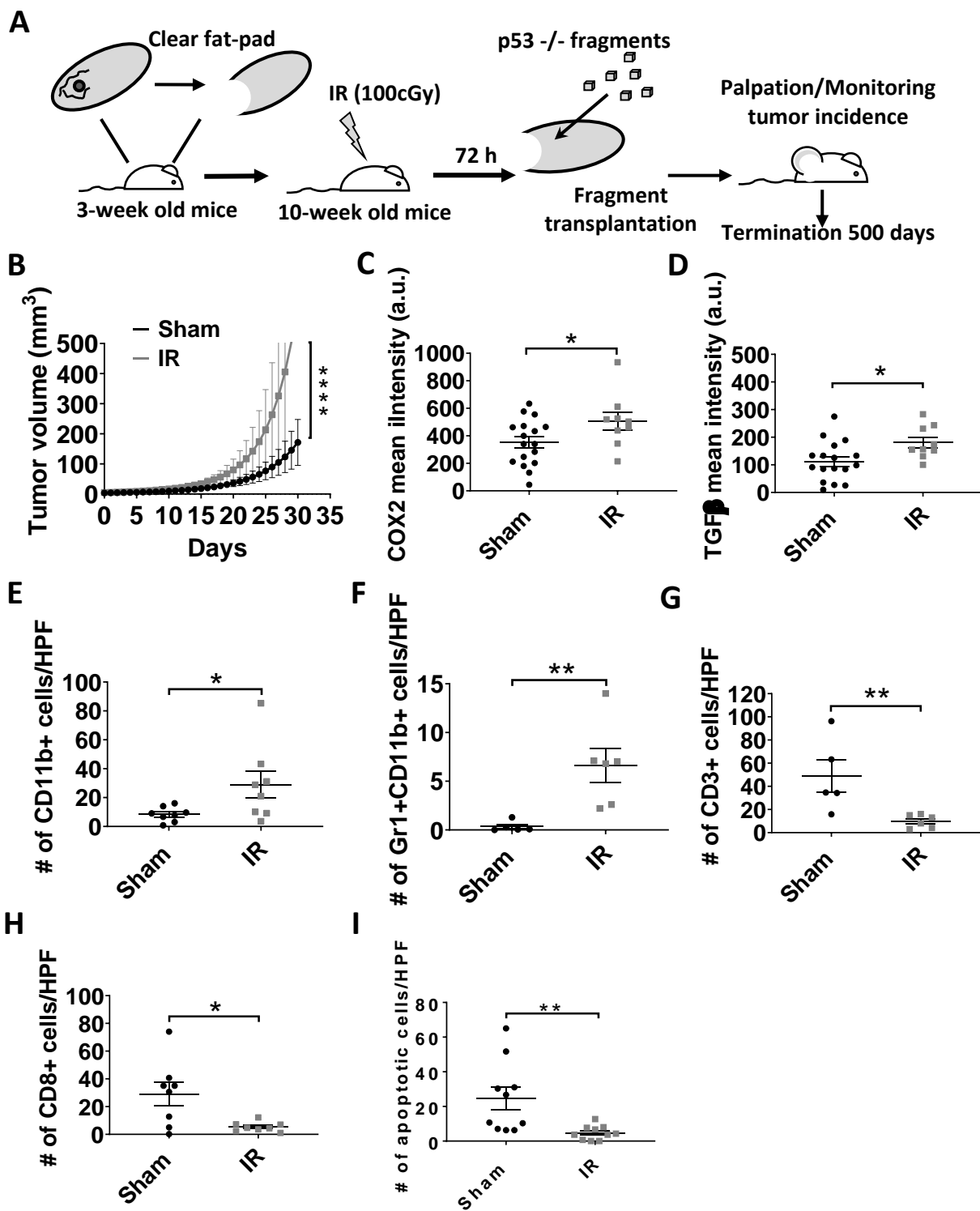


Figure 4

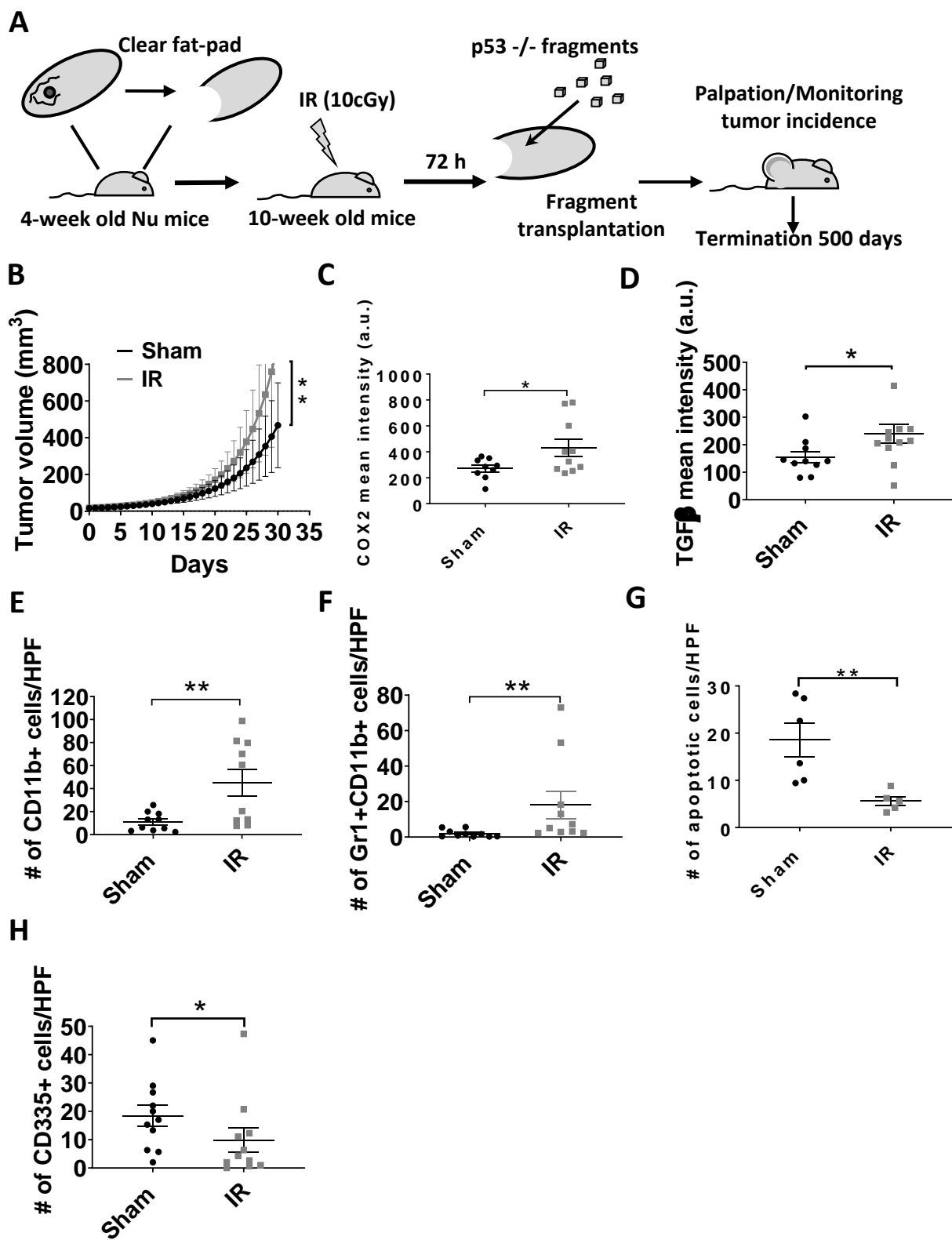


Figure 5

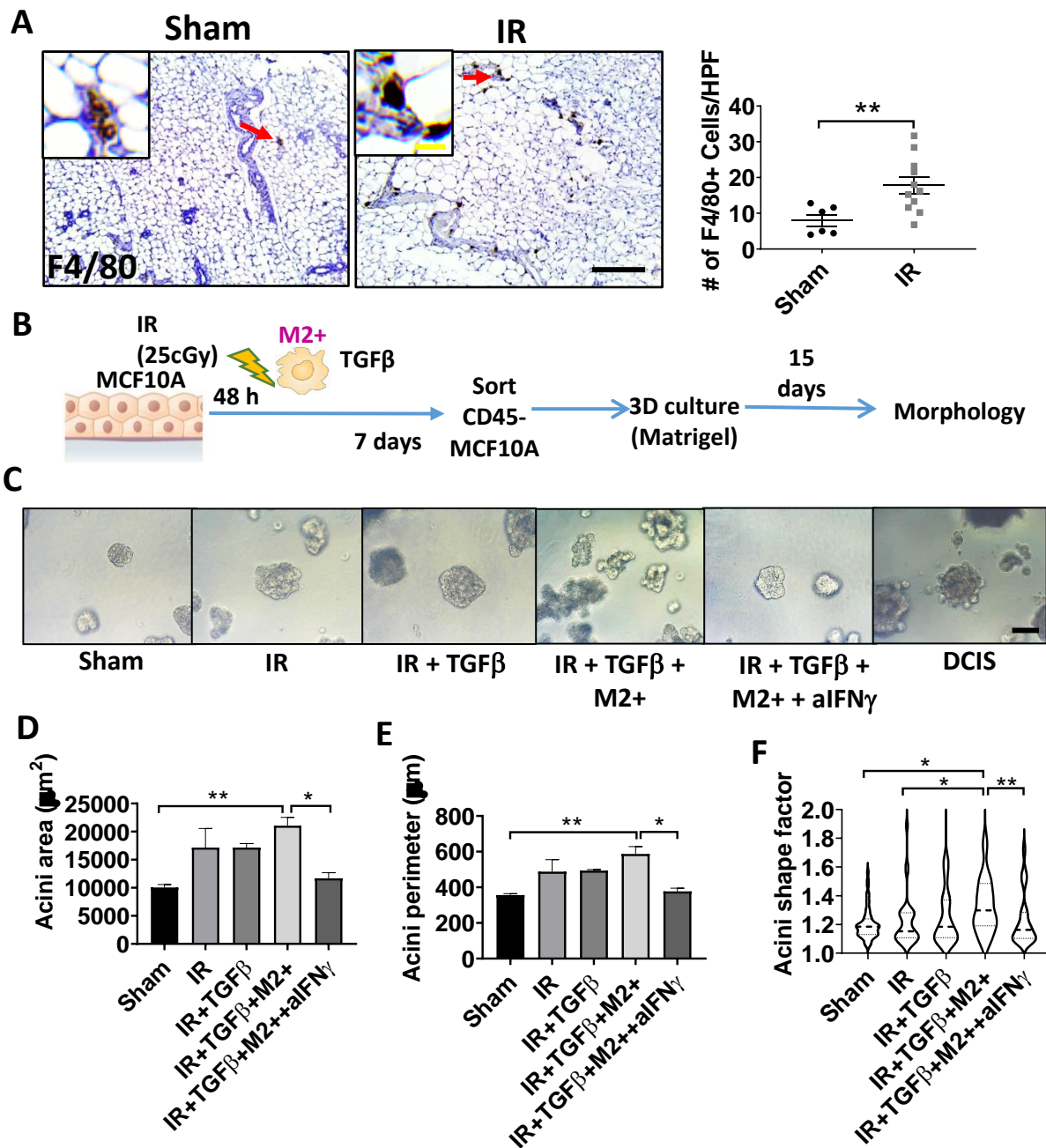


Figure 6

